Acta Crystallographica Section D
Biological Crystallography
ISSN 0907-4449

Pseudo-merohedral twinning in monoclinic crystals of wild-type human brain neuroglobin

Djemel Hamdane,[a] Christophe Lechauve,[b] Michael C. Marden[b] and Béatrice Golinelli-Pimpaneau[a]*

[a]Laboratoire d'Enzymologie et Biochimie Structurales, CNRS, 1 Avenue de la Terrasse, 91190 Gif-sur-Yvette, France, and [b]Inserm U779, Université Paris XI, 78 Rue du Général Leclerc, 94275 Le Kremlin-Bicêtre, France

Correspondence e-mail: beatrice.golinelli@lebs.cnrs-gif.fr

Received 23 October 2008
Accepted 27 January 2009

The purification, crystallization and successful structure determination by molecular replacement of wild-type human brain neuroglobin at 1.8 Å resolution is reported. The apparent space group was orthorhombic $C222_1$, but the real space group was monoclinic $P2_1$, which resulted from twinning. Indeed, the unit-cell parameters, $a = 31.2$, $b = 139.1$, $c = 31.2$ Å, $\beta = 102^\circ$, display a fortuitously close to c and twinning by the operator $l, -k, h$ occurs. Twinning was not evident from the initial analysis of intensity distribution, but pseudo-merohedral twinning was revealed by the Padilla and Yeates test based on local intensity differences. A twinning fraction of 0.5 was determined in *SHELXL*, indicating a perfect hemihedrally twinned crystal. To date, this type of twinning has been reported in more than ten structures, which makes it quite a common case in proteins.

1. Introduction

Neuroglobin (Ngb), a recently discovered intracellular globin in vertebrates (Burmester *et al.*, 2000), is expressed in the brain (Burmester *et al.*, 2000) as well as in other nerve tissues and, with the highest levels, in the retina (Schmidt *et al.*, 2003). The function of Ngb is not fully understood. However, the increase of Ngb expression in neuron cultures upon oxygen deficiency indicates its probable role in the protection of cells against hypoxia (Sun *et al.*, 2003; Greenberg *et al.*, 2008). Ngb may have a myoglobin-like function, supplying the respiratory chain of neuronal mitochondria with oxygen. However, other physiological roles such as electron transfer, peroxidase activity, NO binding or NO detoxification, as observed for other haemoproteins, are also conceivable.

Although analysis of the amino-acid sequence of Ngb reveals little similarity to those of haemoglobin and myoglobin, Ngb shares many of the characteristics of the globins, such as reversible oxygen binding and an overall three-dimensional α-helical globin scaffold (Pesce *et al.*, 2002, 2003). Nonetheless, in the absence of oxygen Ngb displays a particular haem configuration characteristic of a hexacoordinated species, in which the distal and proximal histidines are bound to the Fe atom in addition to the four pyrrole N atoms of the haem (Dewilde *et al.*, 2001; Pesce *et al.*, 2003).

Uniquely in the globin family, human Ngb (NGB) possesses cysteine residues (Cys46 and Cys55 in positions CD7 and D5, respectively) that are capable of forming a disulfide bond which may influence the overall oxygen affinity (Hamdane *et al.*, 2003, 2004). Indeed, it has been shown that NGB can switch between two forms (with low or high affinity for oxygen) depending on the redox state of the cysteines (Hamdane *et al.*, 2003). Although the existence of a disulfide bond has been demonstrated in solution by various biophysical techniques (Hamdane *et al.*, 2003, 2004, 2005; Vinck *et al.*, 2004; Ishikawa *et al.*, 2007), it has not yet been observed by X-ray crystallography, the three-dimensional structure of wild-type NGB being unknown. The reported difficulties in crystallizing wild-type NGB led to mutagenesis and crystallization of an NGB mutant in which Cys46, Cys55 and Cys120 were replaced by Gly, Ser and Ser,

Table 1
Data-collection statistics for wild-type human neuroglobin in different space groups.

Values in parentheses are for the highest resolution shell.

Space group	*P*1	$P2_1$	*C*2	*C*2 (2nd)	$C222_1$
Unit-cell parameters (Å, °)	a = 31.5, b = 31.4, c = 140.9, α = 89.2, β = 90.9, γ = 102.1	a = 31.2, b = 139.1, c = 31.2, $\alpha = \gamma$ = 90, β = 102.0	a = 39.3, b = 48.5, c = 139.2, $\alpha = \gamma$ = 90, β = 90.1	a = 48.5, b = 39.3, c = 139.3, $\alpha = \gamma$ = 90, β = 90.1	a = 39.3, b = 48.5, c = 139.2, $\alpha = \beta = \gamma$ = 90
Resolution	30.76–1.8 (1.9–1.8)	30.50–1.8 (1.89–1.8)	30.53–1.8 (1.89–1.8)	30.56–1.8 (1.89–1.8)	30.53–1.8 (1.89–1.8)
No. of observations	84776	88601	88665	88638	88191
No. of unique reflections	45719	24102	24521	24668	12786
Compleness (%)	93.6 (80.9)	99.5 (96.6)	99.7 (98.0)	99.4 (96.3)	100.0 (100.0)
$\langle I/\sigma(I)\rangle$	5.5 (1.3)	8.6 (2.2)	8.5 (2.1)	9.2 (2.2)	10.9 (2.5)
$R_{\rm merge}$	0.134 (0.623)	0.116 (0.577)	0.113 (0.589)	0.101 (0.589)	0.138 (0.808)
Redundancy	1.9 (1.7)	3.7 (3.4)	3.6 (3.4)	3.6 (3.4)	6.9 (6.6)

Table 2
Molecular-replacement solutions with *Phaser* using data in the resolution range 40–2 Å.

Space group	Molecules in the ASU	LLG†	Clashes	Z‡ rotation	Z‡ translation	Twinned R/$R_{\rm free}$§ (%)
$C222_1$	1	190	8	9.6	11.8	48.3/48.6
*C*2	2	360	16	9.9	8.9	51.1/53.8
				10.4	14.6	
*C*2 (2nd)	2	364	14	11.9	6.5	48.0/50.8
				10.5	14.5	
$P2_1$	2	348	0	9.9	6.8	46.7/48.4
				9.2	13.7	
*P*1	4	564	17	7.8	100	45.6/46.4
				10.4	10.5	
				9.2	15.4	
				8.7	9.1	

† Log-likelihood gain. ‡ Number of standard deviations above the mean. § Before minimization in *SHELXL*.

respectively. In the crystal structure of the NGB mutant at 1.95 Å resolution (Pesce *et al.*, 2003), Gly46 and Ser55 are farther away than expected for a potential disulfide bond in the wild-type protein, strengthening the hypothesis of a major structural rearrangement in the CD loop in wild-type NGB as a result of disulfide-bond breakage/formation between Cys46 and Cys55. This region is directly connected to the E helix, which holds the crucial distal histidine that coordinates the haem. It is clear that the mechanically driven force resulting from the reduction–oxidation of the CD-loop disulfide bond may be transferred to the haem-binding pocket through the E helix (Hamdane *et al.*, 2003, 2004, 2005). This could constitute a potential mechanism by which NGB regulates oxygen binding, which explains the essential role of NGB in oxygen homeostasis of neuronal cells. Therefore, it became urgent to determine the crystal structure of wild-type NGB in order to obtain evidence that the disulfide bond actually forms. Here, we report the crystallization and successful structure determination by molecular replacement of wild-type NGB. The diffraction data exhibit evidence of pseudo-merohedral twinning, in which a $P2_1$ monoclinic crystal emulates *C*-centred orthorhombic symmetry.

2. Materials and methods

2.1. Protein expression and purification

Expression of wild-type NGB was performed as described previously (Dewilde *et al.*, 2001). Ammonium sulfate precipitation (30% and 50%) was used for purification as detailed in Dewilde *et al.* (2008). The ammonium sulfate pellet was dissolved in 50 m*M* Tris–HCl pH 8.5 and dialyzed overnight against the same buffer. Using an ÄKTA purifier system (Amersham Biosciences), the sample was then loaded onto a HiTrap DEAE Sepharose column equilibrated with the same buffer and eluted with 50 m*M* NaCl. The concentrated material was loaded onto a Superose 12 HR 16/50 (Amersham Biosciences). The final purity of the pooled NGB fractions was checked on a 12% SDS–PAGE gel.

2.2. Crystallization

NGB at 10 mg ml^{-1} was crystallized by the hanging-drop procedure in 0.2 *M* magnesium acetate tetrahydrate, 0.1 *M* sodium cacodylate pH 6.5, 20% PEG 8000. Crystals were flash-frozen in a nitrogen stream at 100 K in the same solution containing 25% PEG 8000 and 20% glycerol.

2.3. Data collection and analysis

A data set to 1.8 Å resolution was collected on the PROXIMA1 beamline at the SOLEIL Synchrotron in Saint Aubin (France) and processed with *XDS* (Kabsch, 1993) and *SCALA* (Evans, 2006) (Table 1). The Stanley factor $\langle I^2\rangle/\langle|I|\rangle^2$ and the Wilson's diffraction distribution were obtained from *TRUNCATE* (Collaborative Computational Project, Number 4, 1994).

2.4. Molecular replacement and refinement

Since structure determination by molecular replacement should not be hindered by crystal twinning (Yeates, 1997; Breyer *et al.*, 1999), it was carried out on the $P2_1$ twinned data with *Phaser* (Storoni *et al.*, 2004) using the atomic coordinates of residues 3–45 and 60–149 of the NGB mutant (PDB code 1oj6; Table 2). Self-rotation function analysis of the data processed in space group $P2_1$ using *AMoRe* showed the presence of a twofold axis perpendicular to the crystallographic *b* axis, indicating possible higher (orthorhombic) space-group symmetry or the presence of a noncrystallographic (NCS) axis perpendicular to but not necessarily intersecting the unique *b* axis. The correlation coefficient was 96% in the resolution range 15.0–3.5 Å with a Patterson integration radius of 40 Å.

The initial steps of refinement against intensities were carried out using *SHELXL*97 (Sheldrick, 2008) including the twinning operator (l, $-k$, h) (TWIN), the twin fraction (BASF, initially set to 0.5) and noncrystallographic symmetry (NCS) restraints (NCSY). To calculate $R_{\rm free}$, the test reflections were selected in thin resolution shells; in order to avoid possible correlations introduced by the twinning, all the twin-related pairs belonged to either the test set or the reference set.

3. Results and discussion

3.1. Detection of twinning

Twinning is a crystal-growth anomaly in which two or more crystals intergrow in different relative orientations to form a larger twinned

Table 3
Different cases of pseudomerohedral twinning in monoclinic space groups.

True space group	Pseudo space group	Geometry of unit-cell parameters	Twin operator	Protein
$P2_1$	$P222_1$	$\beta = 90^\circ$	$h, -k, -l$	Cocaine hydrolytic Fab15A10 (Larsen *et al.*, 2002) α-Amino-acid ester hydrolase (Barends & Dijkstra, 2003) PLP-dependent catalytic Fab15A9 (Golinelli-Pimpaneau, 2005)
$P2_1$	$C222_1$	$a = c$	$l, -k, h$	Deoxyhaemoglobin (Ito *et al.*, 1995) 50S ribosomal subunit (Ban *et al.*, 1999) GpD capsid-stabilizing protein of bacteriophage λ (Yang *et al.*, 2000) Orotidine-5′-monophosphate decarboxylase (Wittmann & Rudolph, 2007) Aclacinomycin oxidoreductase (Sultana *et al.*, 2007) Dihaem *c*-type cytochrome DHC2 (Heitmann & Einsle, 2008)
$P2_1$	$C222_1$	$c\cos\beta = -a/2$	$-h, -k, h + l$ or $h, -k, -h - l$	Peroxiredoxin 5 (Declercq & Evrard, 2001) Polymeric immunoglobulin-binding fragment (Hamburger *et al.*, 2004) $\gamma\delta$ T-cell ligand T10 (Rudolph *et al.*, 2004)
$C2$	$F222$	$c\cos\beta = -a/2$	$-h, -k, h + l$	Acetyl coenzyme A synthetase (Lehtiö *et al.*, 2005) THATCH domain of HIP1R (Brett *et al.*, 2006)

aggregate. In pseudo-merohedral twins, the twin operator relating the twin domains belongs to a higher crystal system than the structure. The diffraction spots from the different crystal domains most often completely overlap, so that twinning is not suspected from the diffraction pattern. Pseudo-merohedral twinning can occur in monoclinic crystal systems when the unit-cell parameters meet one of the following conditions: $c\cos\beta = -a/2$, b is close to 90° or a is close to c. Previously reported cases of pseudo-merohedral twinning in a monoclinic space group are listed in Table 3.

The data from the wild-type NGB crystal were processed in space groups $P1$, $P2_1$, $C2$ and $C222_1$ and tested for molecular replacement with *Phaser* (Table 1). Although plausible molecular-replacement solutions were found in the $C222_1$ and $C2$ space groups, they were abandoned because of numerous bad contacts. The space group was assigned as $P2_1$ given the low $R_{\rm merge}$ value, the presence of a twofold screw axis established from analysis of the systematic absences and the success of molecular replacement.

The equality of the a and c parameters, the apparent $C222$ symmetry (as witnessed by the relatively low $R_{\rm merge}$ factor in $C222_1$ and the self-rotation function results) and the high crystallographic R factors after molecular replacement raised the possibility that the crystal was twinned by the twinning operator $(l, -k, h)$, *i.e.* a twofold rotation about the axis diagonal between the a and c monoclinic directions.

Twinning is often detected by an analysis of the second moment of intensities of acentric data $\langle I^2\rangle/\langle|I|\rangle^2$ (Stanley, 1972; Yeates, 1997). A value of 2.0 is expected in the absence of twinning and of 1.5 in the case of a perfect twin. However, the calculated value of 1.972 in *XDS* or 1.99 in *TRUNCATE* for the $P2_1$ NGB data set suggested no twinning at all. Moreover, the observed cumulative intensity distribution of acentric data $N(z) = f(z)$ was only slightly sigmoidal, indicating a low degree of twinning at most (Fig. 1*a*). Another twinning indicator is $\langle|F|^2\rangle/\langle F\rangle^2$, which for acentric data should be 0.785 for untwinned and 0.865 for perfectly twinned data. For wild-type NGB,

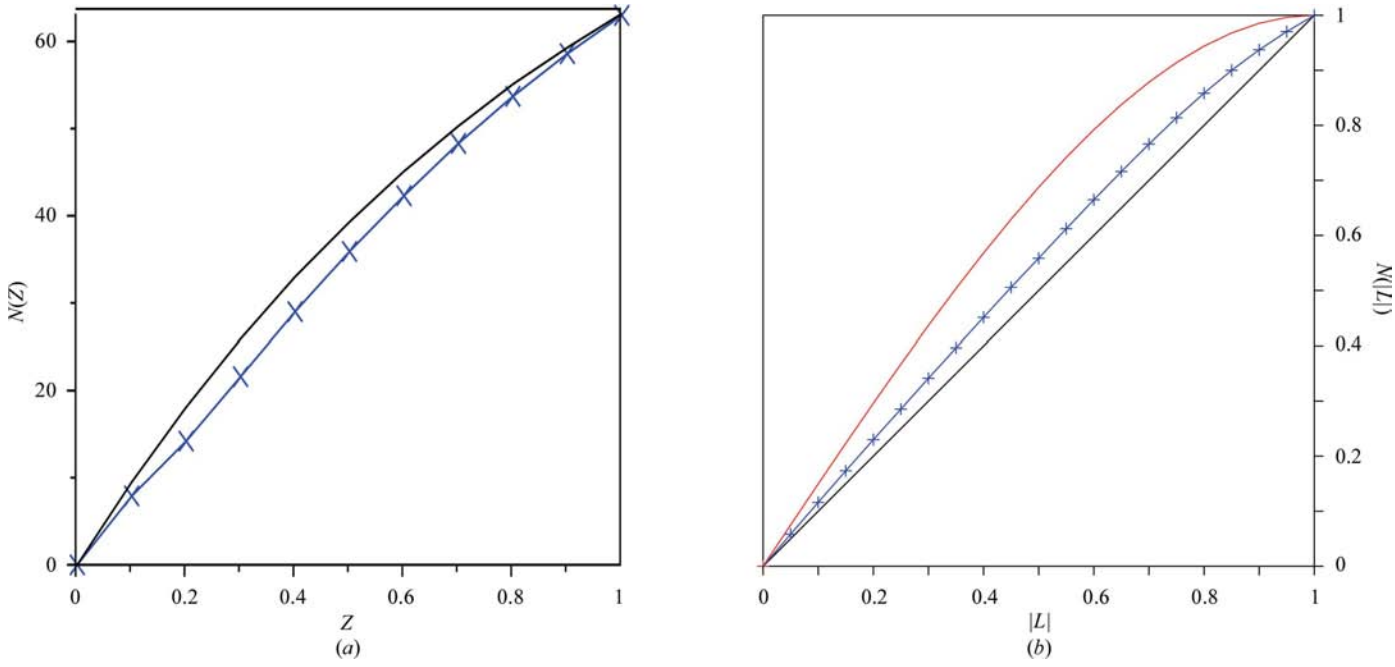

Figure 1
Cumulative intensity distributions. Theoretical distributions for untwinned and perfectly twinned acentric data are shown by black or red curves, respectively. Distributions for observed acentric data are shown by blue lines and crosses. (*a*) The traditional intensity statistics curve, $N(z)$ *versus* z, where $z = I/\langle I\rangle$, gives no clear indication of twinning. (*b*) The local intensity statistics curve, $N(|L|)$ *versus* $|L|$, where $L = [I(h_1) - I(h_2)]/[(I(h_1) + I(h_2)]$ and $I(h_1)$ and $I(h_2)$ are the intensities of the unrelated reflections h_1 and h_2, falls between the curves expected for untwinned and perfectly twinned data.

the value calculated in *CNS* (Brunger, 2007) is 0.834, pointing to the presence of twinning with a high twinning fraction. Discrepancies between the two twinning indicators $\langle I^2\rangle/\langle|I|\rangle^2$ and $\langle|F|^2\rangle/\langle F\rangle^2$ have also been reported in similar cases (Rudolph *et al.*, 2004; Golinelli-Pimpaneau, 2005). Indeed, it is known that the Stanley factor $\langle I^2\rangle/\langle|I|\rangle^2$ can behave abnormally and a newer test based on local intensity differences, which is insensitive to anisotropy and some kinds of pseudo-centring, has been implemented (Padilla & Yeates, 2003). This test was performed for the NGB data set using *DATAMAN* (v.6.3 or above; PY_stats command) from the *RAVE* suite (Uppsala Software Factory). The cumulative probability distribution $N(|L|)$ *versus* $|L|$, where L is defined as $[I(h_1) - I(h_2)]/[I(h_1) + I(h_2)]$ and $I(h_1)$ and $I(h_2)$ are the intensities of the unrelated reflections h_1 and h_2, indeed gave an indication of twinning (Fig. 1*b*). The observed values of $\langle|L|\rangle$ and $\langle L^2\rangle$ were 0.457 and 0.286, respectively, which are between the theoretical values for acentric perfectly twinned data (0.375 and 0.2, respectively) and those for acentric untwinned data (0.5 and 0.333, respectively) (Padilla & Yeates, 2003). When a higher resolution range, also excluding the low signal-to-noise highest resolution data (4–2.5 Å), was considered, the behaviour of the local intensity statistics shifted only slightly towards that for perfect twinning, with observed values of $\langle|L|\rangle$ and $\langle L^2\rangle$ of 0.450 and 0.276, respectively.

3.2. Structure determination using twinned data

The twin fraction was estimated with *SHELXL* using the twin operator $l, -k, h$. The refined twinning fraction of 0.496 is consistent with the low $R_{\rm merge}$ value obtained in space group $C222_1$ but was underestimated by the plots of intensity statistics (Fig. 1), which are only partway towards the curves expected for perfect twinning. This discrepancy has been observed previously and could result from the presence of NCS together with twinning (Rudolph *et al.*, 2004; Golinelli-Pimpaneau, 2005; Wittmann & Rudolph, 2007). When twinning was taken into account, after 40 cycles of Konnert–Hendrickson conjugate-gradient steps the R and $R_{\rm free}$ values dropped to 0.339 and 0.397, respectively, compared with 0.408 and 0.506, confirming the diagnosis of pseudomerohedral twinning. The first steps of model building and refinement in *SHELXL* showed that the electron-density maps are sufficiently clear to allow the building of some missing regions of the model, which provides good evidence that the molecular-replacement solution is correct. However, there was no clear indication that taking twinning into account improves the quality of the map (data not shown). In fact, it is known that twin refinement improves statistics but only occasionally electron density when the twin and NCS axes are almost parallel (Murshudov, 2008), which is the case here. Indeed, the twofold NCS axis relating the two molecules in the asymmetric unit lies in the *ac* plane, perpendicular to the crystallographic *b* axis and almost intersecting it (Fig. 2). The two perpendicular axes generate a third axis perpendicular to them, emulating an orthorhombic unit cell (dashed line in Fig. 2). The geometry of the unit cell allows twinning, since the rotation of the unit cell about the *ac* plane diagonal leads to a superposition of the unit cells, with the interconversion of the *a* and *c* axes and inversion of the *b*-axis direction.

In summary, we report here a new case of a $P2_1$ pseudo-merohedrally twinned crystal, which was observed in wild-type NGB. As frequently observed, twinning occurs in the presence of NCS, with the twofold NCS axis being parallel to one of the twin axes. Interestingly, we have noticed that the density maps were not noticeably improved on including the twin operator, which therefore cannot be a reliable criterion for detecting twinning. In contrast, a significant decrease in the crystallographic factors during refinement when twinning is taken into consideration appears to be a more definitive indicator that the data are twinned.

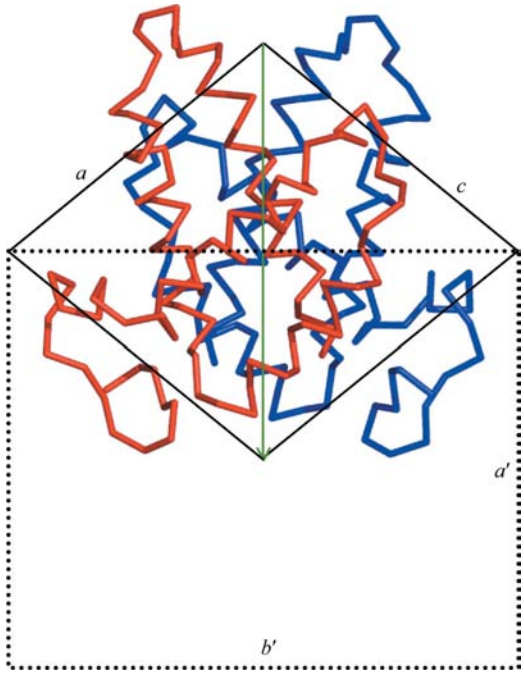

Figure 2
Geometric characteristics of the unit cell. The unit cell (black line) is projected along the *b* axis. The effect of the twinning operator is to emulate pseudo-centring and the resulting $C222_1$ cell $[a' = 2a\cos(\beta/2), b' = 2a\sin(\beta/2), c' = b]$ is indicated as a dashed line. Each of the two NGB molecules (red and blue) in the asymmetric unit are shown as C^α traces and the NCS axis is indicated in green.

This work was supported by the CNRS, INSERM and the University of Paris XI. We thank Professor T. Burmester and T. Hankeln (University of Hamburg/Mainz) for the NGB plasmid, A. Legros for crystallization trials, A. Thompson for help in data collection and R. Herbst-Irmer for advice.

References

Ban, N., Nissen, P., Hansen, J., Capel, M., Moore, P. B. & Steitz, T. A. (1999). *Nature (London)*, **400**, 841–847.
Barends, T. R. M. & Dijkstra, B. W. (2003). *Acta Cryst.* D**59**, 2237–2241.
Brett, T. J., Legendre-Guillemin, V., McPherson, P. S. & Fremont, D. H. (2006). *Nature Struct. Mol. Biol.* **13**, 121–130.
Breyer, W. A., Kingston, R. L., Anderson, B. F. & Baker, E. N. (1999). *Acta Cryst.* D**55**, 129–138.
Brunger, A. T. (2007). *Nature Protoc.* **2**, 2728–2733.
Burmester, T., Weich, B., Reinhardt, S. & Hankeln, T. (2000). *Nature (London)*, **407**, 520–523.
Collaborative Computational Project, Number 4 (1994). *Acta Cryst.* D**50**, 760–763.
Declercq, J.-P. & Evrard, C. (2001). *Acta Cryst.* D**57**, 1829–1835.
Dewilde, S., Kiger, L., Burmester, T., Hankeln, T., Baudin-Creuza, V., Aerts, T., Marden, M. C., Caubergs, R. & Moens, L. (2001). *J. Biol. Chem.* **276**, 38949–38955.
Dewilde, S., Mees, K., Kiger, L., Lechauve, C., Marden, M. C., Pesce, A., Bolognesi, M. & Moens, L. (2008). *Methods Enzymol.* **436**, 341–357.
Evans, P. (2006). *Acta Cryst.* D**62**, 72–82.
Golinelli-Pimpaneau, B. (2005). *Acta Cryst.* D**61**, 472–476.
Greenberg, D. A., Jin, K. & Khan, A. A. (2008). *Curr. Opin. Pharmacol.* **8**, 20–24.
Hamburger, A. E., West, A. P. Jr & Bjorkman, P. J. (2004). *Structure*, **12**, 1925–1935.

Hamdane, D., Kiger, L., Dewilde, S., Green, B. N., Pesce, A., Uzan, J., Burmester, T., Hankeln, T., Bolognesi, M., Moens, L. & Marden, M. C. (2003). *J. Biol. Chem.* **278**, 51713–51721.
Hamdane, D., Kiger, L., Dewilde, S., Green, B. N., Pesce, A., Uzan, J., Burmester, T., Hankeln, T., Bolognesi, M., Moens, L. & Marden, M. C. (2004). *Micron*, **35**, 59–62.
Hamdane, D., Kiger, L., Hoa, G. H., Dewilde, S., Uzan, J., Burmester, T., Hankeln, T., Moens, L. & Marden, M. C. (2005). *J. Biol. Chem.* **280**, 36809–36814.
Heitmann, D. & Einsle, O. (2008). *Acta Cryst.* D**64**, 993–999.
Ishikawa, H., Kim, S., Kwak, K., Wakasugi, K. & Fayer, M. D. (2007). *Proc. Natl Acad. Sci. USA*, **104**, 19309–19314.
Ito, N., Komiyama, N. H. & Fermi, G. (1995). *J. Mol. Biol.* **250**, 648–658.
Kabsch, W. (1993). *J. Appl. Cryst.* **26**, 795–800.
Larsen, N. A., Heine, A., de Prada, P., Redwan, E.-R., Yeates, T. O., Landry, D. W. & Wilson, I. A. (2002). *Acta Cryst.* D**58**, 2055–2059.
Lehtiö, L., Fabrichniy, I., Hansen, T., Schönheit, P. & Goldman, A. (2005). *Acta Cryst.* D**61**, 350–354.
Murshudov, G. N. (2008). *CCP4 School: From Data Processing to Structure Refinement and Beyond*. Argonne National Laboratory.
Padilla, J. E. & Yeates, T. O. (2003). *Acta Cryst.* D**59**, 1124–1130.
Pesce, A., Bolognesi, M., Bocedi, A., Ascenzi, P., Dewilde, S., Moens, L., Hankeln, T. & Burmester, T. (2002). *EMBO Rep.* **3**, 1146–1151.
Pesce, A., Dewilde, S., Nardini, M., Moens, L., Ascenzi, P., Hankeln, T., Burmester, T. & Bolognesi, M. (2003). *Structure*, **11**, 1087–1095.
Rudolph, M. G., Wingren, C., Crowley, M. P., Chien, Y. & Wilson, I. A. (2004). *Acta Cryst.* D**60**, 656–664.
Schmidt, M., Giessl, A., Laufs, T., Hankeln, T., Wolfrum, U. & Burmester, T. (2003). *J. Biol. Chem.* **278**, 1932–1935.
Sheldrick, G. M. (2008). *Acta Cryst.* A**64**, 112–122.
Stanley, E. (1972). *J. Appl. Cryst.* **5**, 191–194.
Storoni, L. C., McCoy, A. J. & Read, R. J. (2004). *Acta Cryst.* D**60**, 432–438.
Sultana, A., Alexeev, I., Kursula, I., Mäntsälä, P., Niemi, J. & Schneider, G. (2007). *Acta Cryst.* D**63**, 149–159.
Sun, Y., Jin, K., Peel, A., Mao, X. O., Xie, L. & Greenberg, D. A. (2003). *Proc. Natl Acad. Sci. USA*, **100**, 3497–3500.
Vinck, E., Van Doorslaer, S., Dewilde, S. & Moens, L. (2004). *J. Am. Chem. Soc.* **126**, 4516–4517.
Wittmann, J. G. & Rudolph, M. G. (2007). *Acta Cryst.* D**63**, 744–749.
Yang, F., Dauter, Z. & Wlodawer, A. (2000). *Acta Cryst.* D**56**, 959–964.
Yeates, T. O. (1997). *Methods Enzymol.* **276**, 344–358.